XFEM and EFG Cohesive Fracture Analysis for Brittle and Semi-Brittle Materials

Yong Guo and C.T. Wu
Livermore Software Technology Corporation
7374 Las Positas Road, Livermore, CA 94551, USA
yguo@lstc.com, ctwu@lstc.com

Abstract

The finite element analysis of dynamic fracture in solids and structures is challenging due to the modeling of arbitrary crack growth in the continuum domain. The well-known mesh size and mesh orientation dependences add more difficulties into the analysis of this type of problems.

In this presentation, we are going to introduce two numerical methods in modeling the dynamic fracture in brittle materials for solid and structures in LS-DYNA®. Both methods were developed by Belytschko and his group [1, 14] and were based on a strong discontinuity approach combined with cohesive forces for the crack initiation and propagation. In EFG method, a visibility method is utilized to define the cracks in the solids and a fast transformation method [18] is applied to handle the boundary conditions in the cracked media. The XFEM method is implemented to model the dynamic fracture in structures. The XFEM method can be viewed as a combination of level sets method and partition of unity method [15] in the description of cracks.

Both academic benchmarks and industrial applications will be presented using these two methods. Advantages and disadvantages will also be discussed.

1 Introduction

Brittle and semi-brittle structures often develop complex fracture and fragmentation patterns during the failure process and the demand for analyzing the fracture pattern and distribution of fragment size has been the focus in many scientific researches such as hypervelocity impact, crashworthiness, explosive drilling. Despite a lot of work has been done in the past to study the physics of fracture and fragmentation patterns, a break-through numerical technology in the failure simulation is still missing. The main difficulty emanates from the inherent multi-scale nature of failure process. For example, the crack initiation and propagation are affected by the presence of flaws at the micro-scale and multiple cracks occur through a complex communication process of stress-wave interactions between them.

In literatures, there are two main ways to numerically model the material failure in brittle and semi-brittle materials. The first one is accomplished by assuming the formation of discrete cracks and zones of local damage in the continuum sense. These damage zones can be represented in a numerical model by means of smeared crack models, where the discrete crack opening is represented by strain concentrations. This approach is often referred to as the weak-discontinuity approach in the continuum damage mechanics (CDM) frameworks. As a result, it leads to the well-known mesh-dependent problem in rate-independent material and certain type of "localization limiter" is required to remedy this numerical defect [4]. In fact, the "localization limiter" forces the localization to occur in a given "volume" instead of a "surface", maintaining the usefulness of existent volumetric dissipation model.

More recently, a strong-discontinuity approach in conjunction with cohesive model is gaining

increasing interest in modeling material failure [9, 10]. This approach is devised to capture the physical discontinuity, i.e. fractures, cracks etc in specific kinematics within finite element or meshfree methods. The cohesive failure is introduced to give the explicit representation of cracks and the ease to handle crack branching and fragmentation. In the creation of new failure surfaces, each opening cohesive zone dissipates a certain amount of cohesive energy and the total energy dissipated in the cracking process is therefore related to the crack path and thus minimize the mesh-dependent problem as seen in CDM.

Meshfree methods are the topic of recent research in many areas of computational science and engineering. One of the early incentives to develop meshfree method was its ability to handle crack propagation problem. Other advantages of the meshfree methods can also be found in many literatures [3, 4, 7]. The first paper utilizes the meshfree technology in the cohesive fracture analysis was given by Klein *et al.* [6]. After that, several meshfree formulations were proposed in the modeling of fracture behaviors. Extended Element Free Galerkin Method (XEFG) was proposed by Rabczuk *et al.* [10] to model three-dimensional cohesive cracks in both statics and dynamics. Zi *et al*. [13] proposed a new way for the crack closure near the tip that does not require crack tip enrichment. Park [9] proposed a modified cohesive model in meshfree fracture analysis.

On the other hand, XFEM is an application of the strong discontinuity approach of the meshfree fracture method to the traditional finite element method. In the extended finite element method, the partition of unity is utilized to incorporate the enrichment functions associated with the crack into the finite elements so that arbitrary cracks can be modeled without remeshing. Discontinuous partitions of unity enrichments were first used to model cracks by Belytschko and Black [19], who used the discontinuous near tip field to model the entire crack for elasto-static problems. In Moes et al. [14] and Dolbow et al. [20], a step function enrichment was developed for elements completely cut by the crack. The approach was generalized to arbitrary discontinuities, including discontinuities in derivatives and tangential values of displacement in Belytschko et al. [21], and was applied to 3-D static problems by Moes and Gravouil [22, 23]. In this method, the discontinuities are completely independent of the finite element mesh: they can cross elements in any manner. Across the discontinuity, they imposed a traction-displacement law, i.e. a cohesive law. The energy dissipation across the discontinuity was chosen to match the energy of fracture.

In this paper, both the meshfree fracture method for solid and the extended finite element method for shell structure fracture are reviewed and implemented in LS-DYNA. They both use the strong discontinuity approach and the cohesive law for the kinematics of the discontinuous crack surfaces. Some benchmarks and industrial applications are used to demonstrate the advantages and disadvantages of the methods.

2 Review of Meshfree Cohesive Fracture Approximation

In contrast to cohesive element method [8] in the fracture analysis where the cohesive surface is defined along the element edge, the representation of crack in the meshfree method is depicted by the so-called “visibility” criterion [2]. The mid-plane cohesive surface in meshfree domain is shown in Figure 1 and is given by

$$\mathbf{x}(\eta) = \sum_{I=1}^{2} \Phi_I^{FEM}(\eta)\mathbf{x}_I + \frac{1}{2}\left(\sum_{J\in\Omega_0^+} \Psi_J(\boldsymbol{X}(\eta))\mathbf{u}_J + \sum_{J\in\Omega_0^-} \Psi_J(\mathbf{X}(\eta))\mathbf{u}_J \right) \tag{1}$$

$$\frac{\partial \mathbf{x}(\eta)}{\partial \eta} = \sum_{I=1}^{2} \mathbf{X}_I \otimes \frac{\partial \Phi_I^{FEM}(\eta)}{\partial \eta} + \frac{1}{2}\left(\sum_{J\in\Omega_0^+} \mathbf{u}_J \otimes \frac{\partial \Psi_J(\mathbf{X})}{\partial \mathbf{X}} + \sum_{J\in\Omega_0^-} \mathbf{u}_J \otimes \frac{\partial \Psi_J(\mathbf{X})}{\partial \mathbf{X}} \right) \frac{\partial \mathbf{X}(\eta)}{\partial \eta} \tag{2}$$

where domains on the upper and lower part of the crack are denoted by Ω_0^+ and Ω_0^-, and are defined in the initial configuration. Eq. (2) is the Jacobian of the cohesive surface parameterization along the mid-plane.

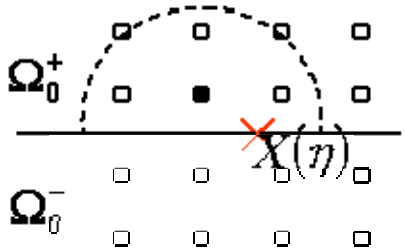

Figure 1: Cohesive surface is defined by meshfree visibility.

3 Review of XFEM Fracture Approximation

In the extended finite element fracture analysis, the cracks are defined by the level set method. The surfaces of discontinuity Γ_α are described by a signed distance function

$$f(\mathbf{x}) = \min_{\bar{\mathbf{x}}\in\Gamma_\alpha} \|\mathbf{x} - \bar{\mathbf{x}}\| sign(\mathbf{n}\cdot(\mathbf{x} - \bar{\mathbf{x}})) \tag{3}$$

where $\bar{\mathbf{x}}$ is a point on the surface of discontinuity Γ_α and $\mathbf{n}$ is a unit normal to the surface of discontinuity. The point $\bar{\mathbf{x}}$ is the closest point to $\mathbf{x}$ and the orthogonal projection of $\mathbf{x}$ on Γ_α. The discontinuity corresponds to $f(\mathbf{x}) = 0$ and the two areas with different signs of $f(\mathbf{x})$ correspond to two domains across the discontinuity, as shown in Figure 2. The approximation close to the discontinuity (the shaded area in Figure 2) consists of two parts: the standard finite element approximation and the enrichment, as in Eq. (4). Eq. (5) shows the enrichment of a step function for cracks cut through the element.

$$\mathbf{u}^h(\mathbf{X}) = \sum_{I=1} \Phi_I^{FEM}(\xi)\mathbf{u}_I + \sum_{I\in w} \Psi_I(\mathbf{X})\mathbf{q}_I \tag{4}$$

$$\Psi_I(\mathbf{X}) = \Phi_I^{FEM}(\xi)\left(H(f(\mathbf{X})) - H(f(\mathbf{X}_I))\right) \tag{5}$$

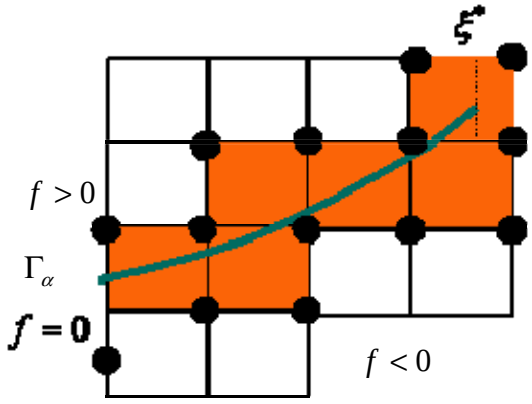

Figure 2: Cohesive surface is defined by level set in XFEM.

4 Initially-rigid Cohesive Law

Many cohesive models belong to the type of initially-elastic cohesive law where the effective Young's modulus is dependent of model refinement and the results are not convergent. In the initially-rigid cohesive law, the cohesive surface is only introduced as needed. Therefore, correct wave speeds can be captured before any crack occurs. In this study, we adopted a modified cohesive law [11] for the crack initiation and propagation in both EFG and XFEM method. A linear initially-rigid cohesive law is shown as in Figure 3.

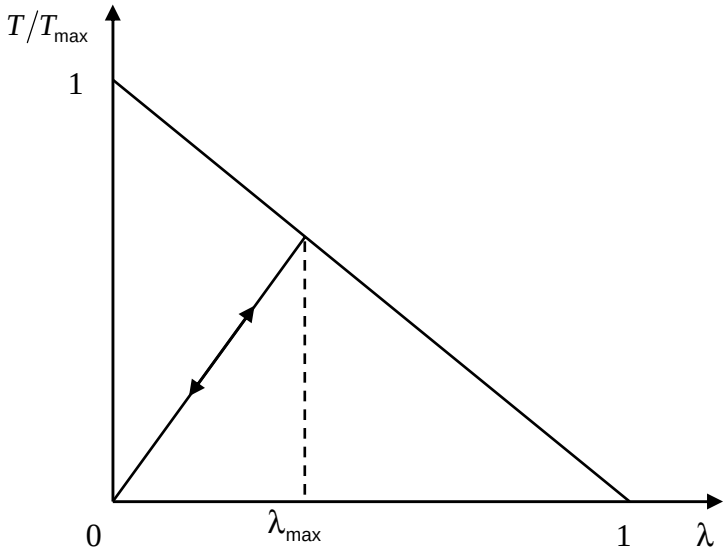

Figure 3: Initially rigid cohesive law.

The displacement jump λ is defined by

$$\lambda = \sqrt{\left(u_n / (\delta_{0n} + \delta_n)\right)^2 + \beta^2 \left(u_t / (\delta_{0t} + \delta_t)\right)^2} \tag{6}$$

where u_n and u_t are crack opening displacements in normal and tangential directions obtaining from Eq. (1) in EFG and Eq. (4) in XFEM. The material constants involved in Eq. (6) include:

δ_n and δ_n are critical values at which crack takes place in normal and tangential directions respectively, δ_{0n} and δ_{0t} are regularization parameters that are introduced to prevent the time-discontinuity and thus eliminate the numerically instability [11]. α is the parameter coupling normal and shear tractions and λ_{cr} is the critical displacement jump. The corresponding normal traction and tangential traction are obtained by the standard cohesive relationships by following

$$T_{efs} \equiv \sqrt{T_n^2 + \left(\frac{\beta}{\alpha}\right)^2 T_t^2} = T_{\max} \tag{7}$$

$$T_n = \frac{1-\lambda}{\lambda}\frac{u_n}{\delta_n}\frac{T_{\max}}{1-\lambda_{cr}} \quad \text{and} \quad T_t = \frac{1-\lambda}{\lambda}\frac{u_t}{\delta_t}\frac{\alpha T_{\max}}{1-\lambda_{cr}} \tag{8}$$

where T_n is the normal traction, T_t is the tangential traction and T_{max} is the maximum normal traction that the crack surface can bear before failure. Note that the cohesive tractions are defined on an un-deformed area per unit.

Accordingly, the nodal forces follow from the tractions can be obtained by the surface integration along the crack surface. The implementation flow chart of the initially-rigid cohesive law is shown in Figure 4.

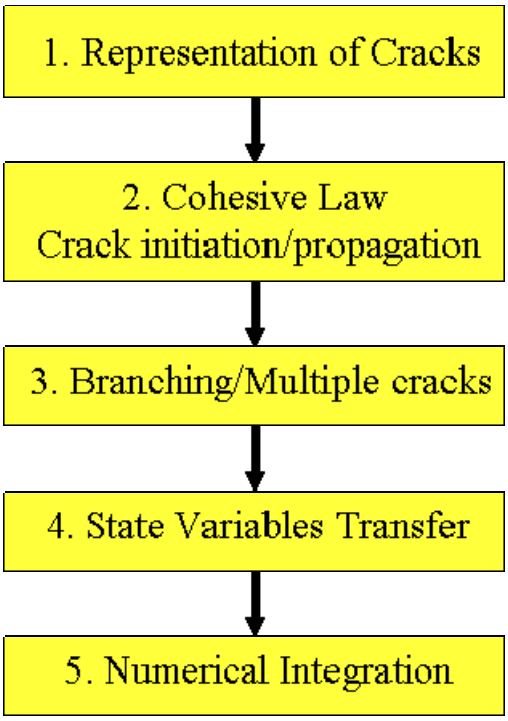

Figure 4: Flow chart for crack initiation and propagation using initially-rigid cohesive law.

The final discrete equations can be derived in a standard fashion and given by

$$\boldsymbol{f}^{kin} = \boldsymbol{f}^{\text{int}} - \boldsymbol{f}^{ext} + \boldsymbol{f}^{coh} \tag{9}$$

$$\boldsymbol{f}_e^{kin} = \int_{\Omega_0^e} \rho_0 \boldsymbol{N}^T \boldsymbol{N} H((-1)^e f(\boldsymbol{X})) d\Omega_0^e \ddot{\boldsymbol{u}} \tag{10}$$

$$\boldsymbol{f}_e^{int} = \int_{\Omega_0^e} \boldsymbol{B}^T \sigma H((-1)^e f(\boldsymbol{X})) d\Omega_0^e \tag{11}$$

$$\boldsymbol{f}_e^{ext} = \int_{\Omega_0^e} \rho_0 \boldsymbol{N}^T \boldsymbol{b} H((-1)^e f(\boldsymbol{X})) d\Omega_0^e + \int_{\Gamma_{0,t}^e} \boldsymbol{N}^T \boldsymbol{t} H((-1)^e f(\boldsymbol{X})) d\Gamma_{0,t}^e \tag{12}$$

$$\boldsymbol{f}_e^{coh} = (-1)^e \int_{\Gamma_{0,t}^e} \boldsymbol{N}^T \boldsymbol{\tau}^c \boldsymbol{n}_0 d\Gamma_{0,t}^e \tag{13}$$

5 Numerical Examples

5.1 Edge-cracked plate under impulsive loading

Next we simulate an experiment reported by Kalthoff and Winkler [16] in which a plate with two initial edge notches is impacted by a projectile. The experiment is shown in Figure 5. In the experiment at low strain rate, brittle failure with a crack propagation angle of about 70° is observed [16].

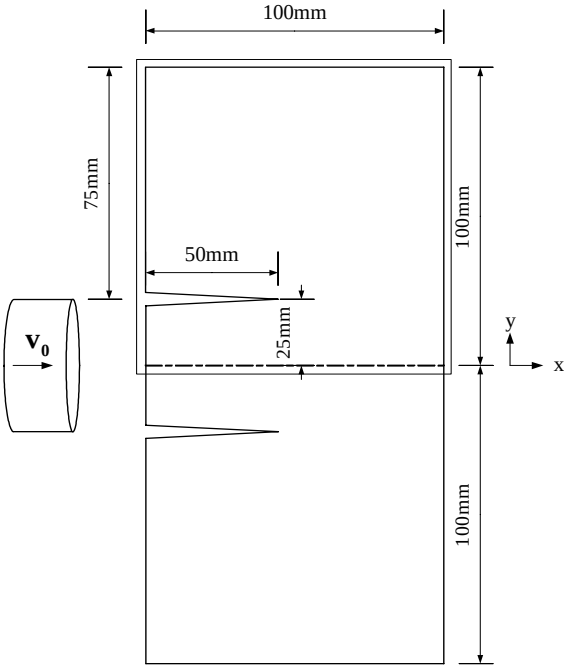

Figure 5: Experimental set-up for edge-cracked plate under impulsive loading; only half of the plate is modeled.

Due to the twofold symmetry of the configuration, only the upper half of the plate is modeled: At the bottom edge of the finite element model, $u_y = 0$ and $t_x = 0$. The initial impact velocity is applied on the left edge on the segment $0 \le y \le 25\text{mm}$. We assumed that the projectile has the

same elastic impedance as the specimen, so we applied one half of the projectile speed, 16.5m/s for the brittle fracture mode, to the left edge as an initial condition. The initial notch was modeled by including two lines of nodes separated by 0.3mm. The material is a maraging steel 18Ni1900 and its material properties are $\rho = 8000\text{kg/m}^3$, E=190GPa and $\nu = 0.30$ [17]. We used a central difference time integration scheme with a Courant number of 0.1. We found that a low Courant number is necessary for the elements which contain a discontinuity.

A cohesive crack model with fracture energy $G_F = 2.213\times10^4\,\text{N/m}$ and $\delta_{\max} = 5.245\times10^{-5}\,\text{m}$ and a linear cohesive law was used. For the crack initiation criterion, we used the maximum tensile stress criterion. Numerical simulation was made with a 50x50 mesh shown in Figure 6. Both the meshfree method and the XFEM are used to solve the problem.

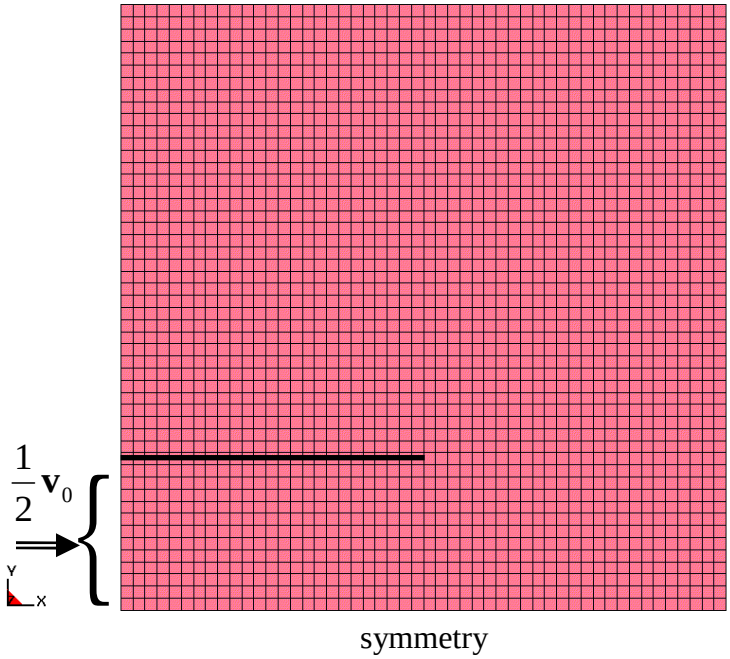

Figure 6: 50x50 mesh with pre-crack.

The result of crack path from XFEM is shown in Figure 7. The average angle from the initial crack tip to the final crack tip is about 62.5° and the initial crack angle is about 67.5°; the crack path is nearly straight. This angle is smaller than the observed angle [16] and the angle obtained by mesh-free methods.

The crack path from EFG fracture method is shown in Figure 8. The average crack angle is about 69.0°, very close to the experiment observation. The accurate result is partially because of the higher approximation order of the meshfree method.

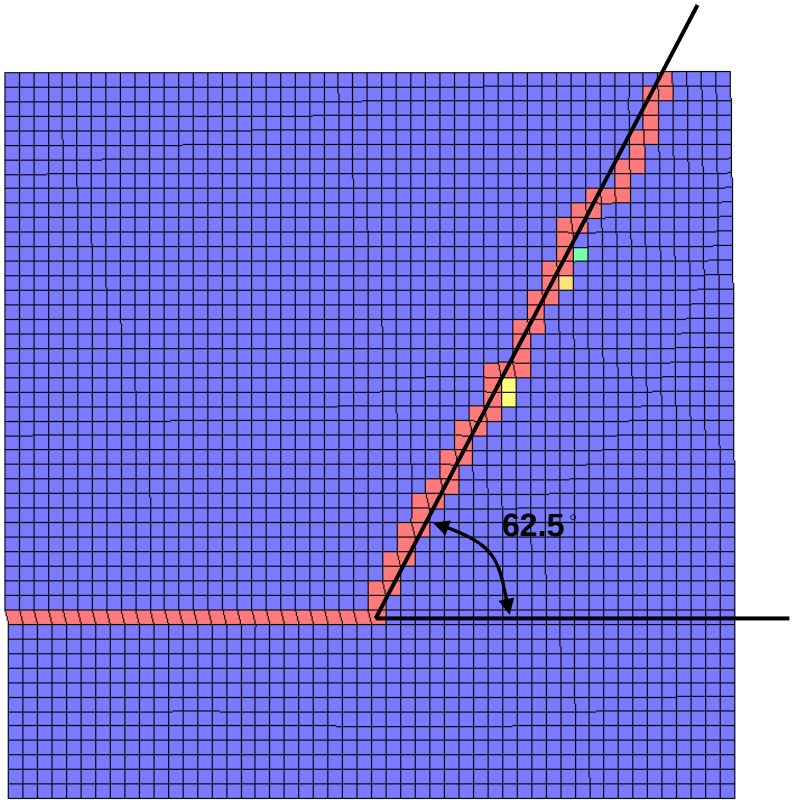

Figure 7: Crack path by XFEM.

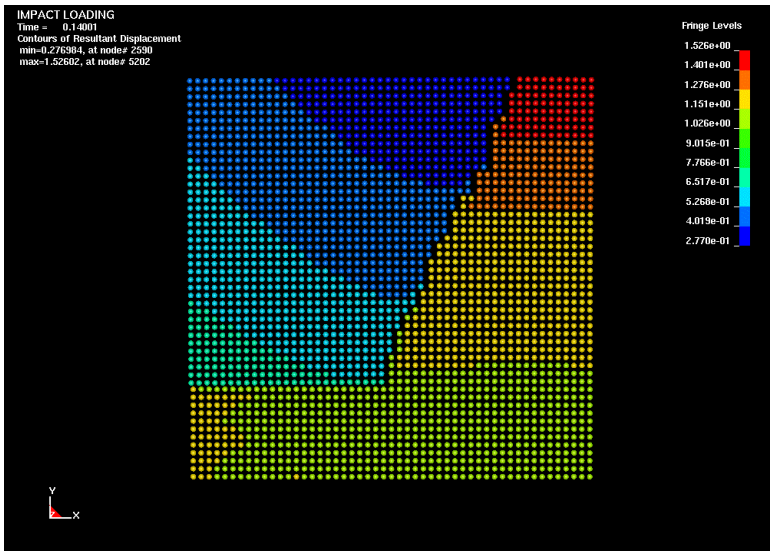

Figure 8: Final crack path by EFG.

5.2 A notched plate under bending test

In this example, a brittle fracture of thick plate under bending is simulated. This classical problem of a single-edged notched plate supported in two points is shown in Figure 9. The

problem is simulated using EFG method. The material properties of the plate are given in non-dimensional unit, Young's modulus = 7.16e+04, Poisson's ratio = 0.23, density = 2.e4-09, mode I energy release rate = 0.25 and the critical displacement jump = 0.0001 with the corresponding maximum normal traction = 500.

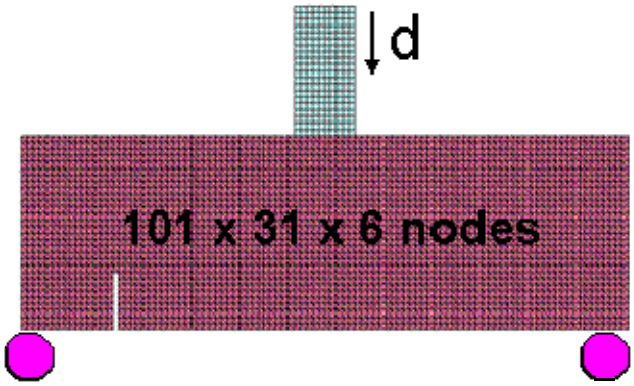

Figure 9: Single-edged notched plate under bending.

Figure 10 shows the final crack patch in a resultant displacement plot. The result demonstrates the capability of the presented method to model a curved crack.

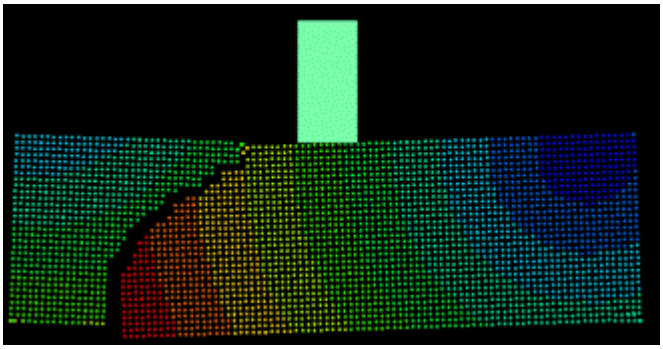

Figure 10: Final crack path.

5.3 Cylinder shell under pulling

The last example is a thin cylinder shell with a pre-crack under axial pulling. The right end of the shell is fixed and the left end is pulled with a velocity of $\mathbf{V} = 5\text{mm}/\mu\text{s}$, as shown in Figure 11. The material is kinematic plastic with $\rho = 7.83\times10^{-6}\text{kg/mm}^3$, E=70GPa, $\nu = 0.30$ and $\sigma_y = 0.1\text{GPa}$, $E_p = 0.2\text{GPa}$. The fracture energy release rate is 50kN/m and the cohesive law parameters are: $\sigma_{\max} = 0.2\text{GPa}$ and $\delta_c = 0.5\text{mm}$.

The problem is solved with two meshes: a coarse mesh with 1860 elements and a fine mesh with 7440 elements. The crack positions at different times with the fine mesh are shown in Figure 12.

Figure 13 shows the comparison of the resultant pulling force obtained using the two meshes. The fine mesh yields smoother force curve than the coarse mesh.

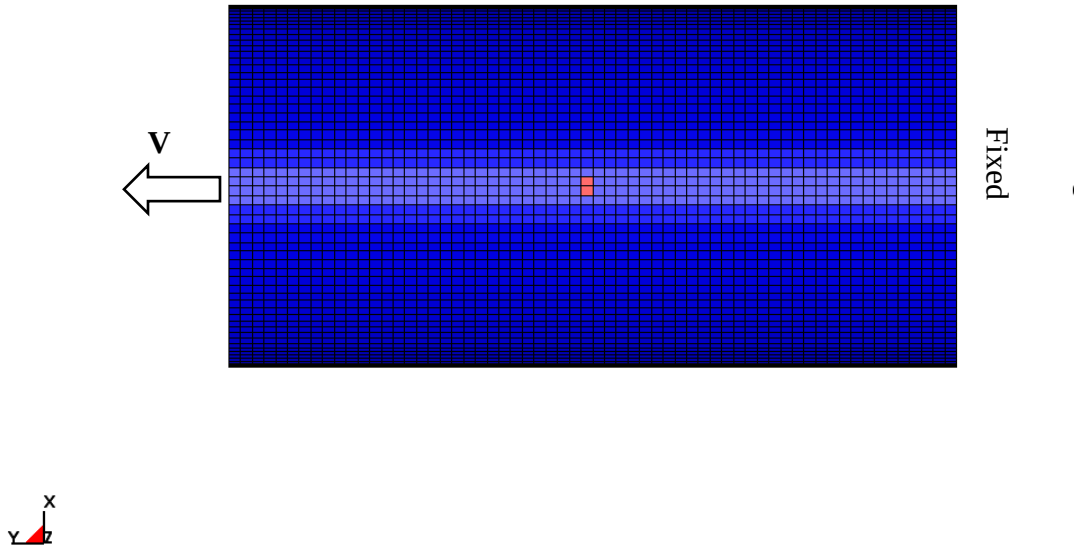

Figure 11: Cylinder shell under pulling.

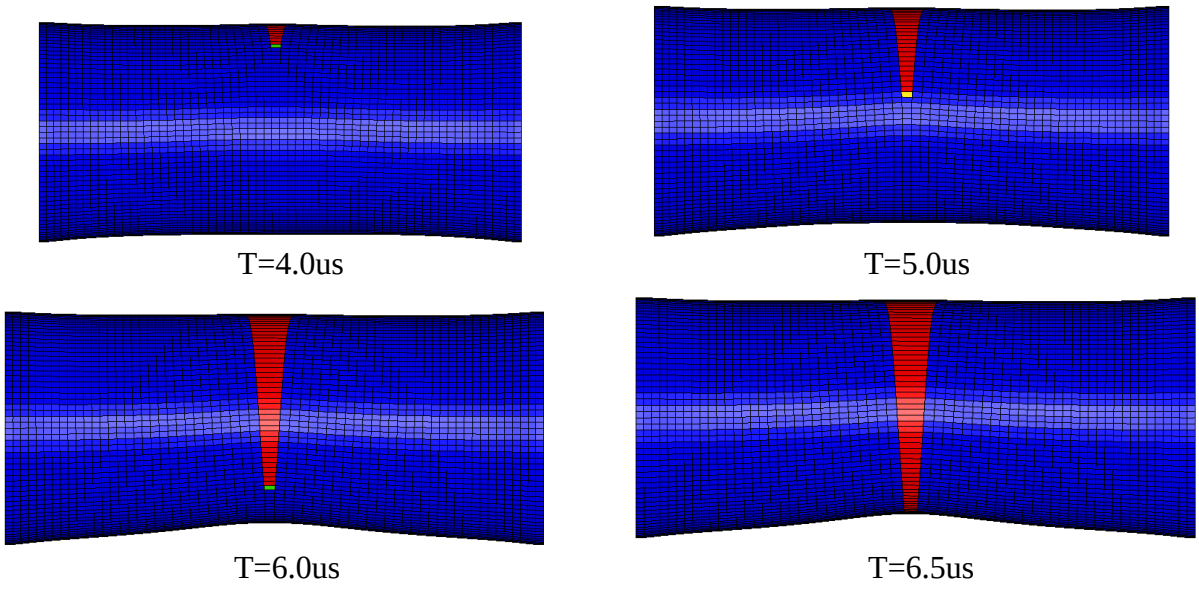

Figure 12: Crack propagation at different times.

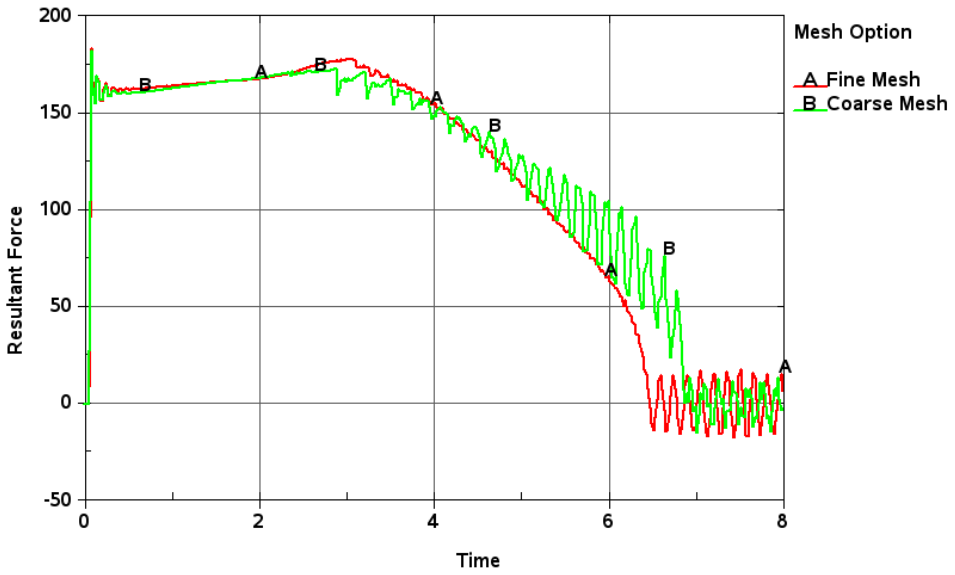

Figure 13: Comparison of resultant pulling force using two meshes.

6 Conclusion

The meshfree fracture method for solids and the extended finite element method for shell structures are presented in this paper and implemented in LS-DYNA. The two methods use the strong discontinuity approach to model the cracks and the cohesive zone model for the fracture kinematics. Both methods show their possibilities to model dynamic fracture with arbitrary cracks and without remeshing. Currently these methods are better fitted to model cracks in brittle and semi-brittle materials. Several issues which are not addressed in this paper such as the treatment of multiple cracks, responses from different crack initiation and propagation criteria, the ability to model contact between debris and crack closure problems will be further investigated.

References

1. Belytschko, T. and Tabbara, M., "Dynamic fracture using element-free Galerkin methods," International Journal for Numerical Methods in Engineering, 39, 923-938, 1996.
2. Belytschko, T., Lu, Y. Y., and Gu, L., "Element-free Galerkin methods", International Journal of Numerical Methods in Engineering, 37(2), 229-256, 1994.
3. Belytschko, T., Krongauz, Y., Organ, D., Fleming, M. and Krysl, P., "Meshless methods: An overview and recent developments", Computer Methods in Applied Mechanics and Engineering, 139, 3-47, 1996.
4. Chen, J. S., Pan, C., Wu, C. T. and Liu, W. K., "Reproducing kernel particle methods for large deformation analysis of non-linear structures", Computer Methods in Applied Mechanics and Engineering, 139, 195-227, 1996.
5. Chen, J.S., Wu, C. T., Belytschko, T., "Regularization of material instabilities by meshfree approximation with intrinsic length scales", International Journal of Numerical Methods in Engineering, 47, 1303-1322, 2000.
6. Klein, P. A., Foulk, J. W., Chen, E. P., Wimmer, S. A. and Gao, H. J., "Physical-based modeling of brittle fracture: cohesive formulations and the application of meshfree methods", Theoretical and Applied Fracture Mechanics, 37, 99-166, 2001.
7. Li, S. and Liu, W. K., "Meshfree and particle methods and their applications", Applied Mechanics Reviews, 55, 1-34, 2002.
8. Ortiz, M. and Pandolfi, A., "Finite-deformation irreversible cohesive elements for three-dimensional crack-propagation analysis", International Journal for Numerical Methods in Fluids, 44, 1267-1282, 1999.

9. Park, C. K., "The development of a generalized meshfree approximation for solid and fracture analysis" Ph.D. thesis dissertation, The George Washington University, U.S.A., 2010.
10. Rabczuk, T., Belytschko, T., "A three-dimensional large deformation meshfree method for arbitrary evolving cracks", Computer Methods in Applied Mechanics and Engineering, 196, 2777-2700, 2007.
11. Sam, C. H., Papoulia, K. D. and Vavasis, S.A., "Obtaining initially-rigid cohesive finite element models that are temporally convergent", Engineering Fracture Mechanics, 72, 2247-2267, 2005.
12. Zavattieri, P. D. and Espinosa, H. D., "Grain level analysis of ceramic microstructures subjected to normal impact loading", Acta Materialia, 49(20), 4291-4311, 2001.
13. Zi, G, Rabczuk, T. and Wall, W., "Extended meshfree methods without branch enrichment for cohesive cracks", Computational Mechanics, 40, 367-382, 2007.
14. Moes, N., Dolbow, J., Belytschko, T., "A finite element method for crack growth without remeshing," International Journal for Numerical Methods in Engineering, 46: 131-150, 1999.
15. Babuska, I. and Melenk, J.M., "The partition of unity method," International Journal for Numerical Methods in Engineering, 40:727-758, 1997.
16. Kalthoff, J.F. and S. Winkler, S., Failure mode transition at high rates of shear loading, *International Conference on Impact Loading and Dynamic Behavior of Materials*, 1:186-195, 1987.
17. Decker, R.F., Source Book on Maraging Steels, American Society for Metals, 1979.
18. Wu, C.T. and Lu, H.S., "Practical fast meshfree analysis," U.S. Patent, 2009.
19. Belytschko, T. and Black, T., "Elastic crack growth in finite elements with minimal remeshing," *International Journal for Numerical Methods in Engineering*, 45:601–620, 1999.
20. Dolbow, J., Moes, N., and Belytschko, T., "Discontinuous enrichment in finite elements with a partition of unity metho," *Finite Element Analysis and Design*, 36(3):235–260, 2000.
21. Belytschko, T., Mo¨es, N., Usui, S. and Parimi, C., "Arbitrary discontinuities in finite element. *International Journal of Numerical Methods in Engineering*," 50(4):993–1013, 2001.
22. Mo¨es, N., Gravouil, A. and Belytschko, T., "Non-planar 3d crack growth by the extended finite element and level sets. part i: Mechanical model," *International Journal of Numerical Methods in Engineering*, 53:2549–2568, 2002.
23. Gravouil, G., Mo¨es, N. and Belytschko, T., "Non-planar 3d crack growth by the extended finite element and level sets. part ii: level set update," *International Journal of Numerical Methods in Engineering*, 53:2569–2586, 2002.